Proceedings of Aerospace Europe Conference 2020 (AEC2020), 24-28 February 2020,
Bordeaux, France. Paper number 00337

00260

AN AUTOMATED APPROACH FOR THE AERODYNAMIC DESIGN OF CLOSE-COUPLED PROPULSION/AIRFRAME CONFIGURATIONS

Jesús Matesanz-García [(1)], Robert Christie [(2)], Fernando Tejero[(3)], David MacManus[(4)], and Alexander Heidebrecht [(5)]

[(1)]Cranfield University Propulsion Engineering Centre, Cranfield, Bedfordshire, UK. Email: Jesus.Matesanz-Garcia@cranfield.ac.uk,
[(2)(3)(4)(5)] Cranfield University Propulsion Engineering Centre, Cranfield, Bedfordshire, UK.

KEYWORDS: Novel aircraft configurations, boundary layer ingestion, propulsive fuselage, aerodynamic performance, Class Shape Transformations, CFD, Design Space Exploration, multi-objective optimizations, genetic algorithm

ABSTRACT:

Reducing aircraft emissions is a key element in mitigating the environmental impact of aviation. Within this context, different novel aircraft propulsion configurations have been proposed. A common feature of many of these novel configurations is the closer integration of the propulsive system and the aircraft airframe with an expected increase of the aerodynamic coupling. Therefore, is necessary to assess the performance of the aerodynamic installation of the propulsive system of these configurations with a systematic approach.

A systematic and automated methodology for the design and performance evaluation of embedded propulsion systems is defined. This methodology is demonstrated with a Boundary Layer Ingestion propulsive fuselage concept. This approach covers the geometry design of the selected configuration, an automatic aerodynamic numerical computation and a novel performance evaluation for the design. A Design Space Exploration was performed to characterize the relative importance of the individual parameters of the geometry and their correlation with the key performance metrics. Finally, a multi-objective optimization was carried to demonstrate the capabilities of this approach.

1. INTRODUCTION

1.1. Background

Reducing aircraft emissions is seen as a key element in mitigating the environmental impact of aviation. National governments and international agencies have committed to reduce the net aviation CO2 emissions by 50% for the year 2050, based on 2005 levels [1]. This reduction of the emissions can be partially achieved by the increase of the propulsive efficiency, the application of aerodynamic improvements to reduce the overall aircraft drag, or the reduction of the total weight of the system. Within this context, different novel aircraft propulsion configurations have been proposed [2–4]. A common feature of many of these novel configurations is the closer integration of the propulsive system with the aircraft airframe. Hence, an increase of the aerodynamic coupling is expected for these novel configurations. To assess the viability of these novel integrated propulsive systems it is vital to evaluate the effect of the propulsion-airframe interactions on the aerodynamic performance of the installation.

Traditionally, the different elements of the aerodynamic installation of the propulsive system (intake, nacelle and exhaust) have been analysed and designed separately [5–7]. However, the closer coupling between the airframe and the propulsive system of the novel configurations requires the analysis of the installation as whole. Thus, it is necessary to evaluate the effect of the interaction of the different elements of the installation and with the airframe for each of the novel configurations. To develop the highly integrated concepts it is essential to study the requirements of the future installation architectures. Intake, nacelle and exhaust characteristics must be studied to determine the impact on the aerodynamic performance of the novel aircraft configurations.

As a consequence of the closer integration of the propulsion system, an increased level of intake distortion is expected. Accordingly, previous research on installation aerodynamics has mainly focused on intake design. Optimization of the intake has been investigated for highly integrated intakes for Blended Wing Body configurations by Rodríguez [8] and Kim et al. [9]. Similarly, Kenway et al. [10] optimized a STARC-ABL BLI propulsor intake for minimum distortion. Some numerical studies have been carried out for the full installation of different configurations such as the STARC-ABL [11]. Nevertheless, there is a lack of work on the effect of

the nacelle and exhaust design, and the interaction of the whole installation. A direct effect of the strong coupling between the airframe and the propulsion system is that the conventional performance analysis methodologies could no longer be applying. Consequently, it is necessary to revise the methodologies for the requirements of the novel systems. This challenge requires the application of a novel systematic approach for the design and analysis of the configurations for different flight conditions. This includes aspects such as the design of an integrated intake, cowl and exhaust system. It is essential to develop a methodology to evaluate the effect of the aerodynamic installation on the performance of the propulsive system of these new configurations.

1.2. Aircraft configuration

The growing number of novel aircraft concepts with different characteristics complicates the development of a common approach. Therefore, it is necessary to bound the configurations into groups with similar characteristics and target each of them with a consistent methodology. The main relevant novel technologies proposed to date can be broadly divided into two groups. The first group comprises disruptive aircraft layout systems. In this group are airframe concepts such as the Blended Wing Body [8,12]. The second group comprises concepts that keep the conventional tube and wing configuration [10,11,13–15]. The second group is of particular interest, because some of the novel characteristics proposed could be applied to existing aircraft designs without a redesign of the full airframe. Therefore, it is of interest to provide an assessment of the performance of this group of configurations and to investigate the potential benefits and limitations.

Within both groups, a common concept is the Boundary Layer Ingestion (BLI) [11,13,16]. The main idea behind these configurations is the improvement of the aerodynamic performance of the aircraft by ingesting a fraction of the airframe boundary layer with a propulsion system and filling with the jet the momentum deficit of the wake of the aircraft [17–19].

The main challenge on the design of these new configurations is the change of the conventional location of the propulsion system in favour of a closer integration with the airframe. Highly integrated positions closer to the fuselage are preferred to reduce its drag contribution. However, the installation design must reduce the penalties from the embedded system such as the additional drag generation or the increase in distortion levels at the fan face. Consequently, a new design methodology is required that can assess the intake, nacelle and exhaust aerodynamics for these new close coupled configurations. This is the main aim of the current work.

The potential benefits of BLI configurations have been addressed by Smith [19], Felder et al. [12], Hall et al. [17], Blumenthal et al. [20], and Uranga et al. [18]. Most of the work focused on the potential performance and power saving benefit of the BLI configurations. However, besides the intake performance analysis, the importance of the aerodynamic installation of the full propulsive system has been neglected. Nacelle and exhaust design can have a fundamental effect on the overall system aerodynamic performance. Additionally, the highly embedded configurations need to minimize the intake distortion without penalising the aerodynamic performance of the propulsor. Thus, a multi objective approach is required for the study of the aerodynamic installation performance.

As a case study for the installation aerodynamic design, a fuselage based BLI system similar to previous studies [11,14,15]. This concept is based on an annular propulsor positioned on the fuselage aft section. For the study, a 2D axisymmetric model of the BLI propulsor is implemented on a medium-sized single-aisle aircraft.

1.3. Scope of this work

The aim of this work is to demonstrate a methodology for the design of the propulsion system installation and airframe integration for close-coupled configurations. Therefore, a systematic automated approach has been developed for the geometry generation, CFD modelling and aerodynamic performance evaluation. This methodology is designed to provide an appropriate environment to perform Design Space Explorations (DSE) and optimizations. The development of this approach was based on the following stages:

1. Revision of the aerodynamic performance evaluation method for the novel concepts
2. Development of a geometry design methodology for the aerodynamic installation of a BLI propulsive fuselage configuration. The methodology will be based on the use of Class Shape Transformations (CST) [5,21–23]
3. Generation of an automated CFD methodology for the axisymmetric designs
4. Design Space Exploration (DSE) for a particular propulsor installation location
5. Optimization methodology development applying a genetic algorithm

2. Thrust-drag bookkeeping and performance evaluation

2.1. Thrust and drag bookkeeping

Drela [24] proposed the Power Balance Method which has been used to evaluate the performance of novel configurations. Uranga et al. [25] applied this methodology for a boundary layer ingestion aircraft based on experimental wind tunnel data, while Hall et al. [17] applied this methodology for the same configuration with a numerical approach. Arntz et al. [26] applied an Exergy Analysis to a Blended Wing Body BLI configuration. Some of the main advantages of these methodologies are the decoupling between the propulsive efficiency and the fan efficiency [20], and the capability to study the behaviour of the aerodynamic performance for close coupled systems without separating the different regions of the flow. However, these approaches require a notable computational effort since their control volume requires a detailed discretization of the far field regions. In addition, there is not a clear benchmark to compare the results of the power-based methods; and the experimental results necessary for validation are scarce. Thus, it is necessary to reassess the use of more conventional methodologies for the thrust and drag bookkeeping, and adapt them for the close-coupled systems.

A Modified Near-Field Thrust and Drag accounting methodology (Fig. 1) is proposed based on the AGARD 237 [27]. A clear advantage of this methodology comes from excluding the post exit terms in the analysis. This avoids the evaluation of the interaction between the aircraft wake and the propulsor jet [26]. The pre-entry force terms, ϕ_{pre}, can be defined by applying a force balance to the control volume (Eq. 1) for the flux surface forces, *F,* and the wall surface forces, *θ*. The value of the upstream capture plane, F_{G0}, can be derived analytically for a given fan mass flow and flight conditions. The main metric coming from this analysis is the Net Vehicle Force, *NVF*, (Eq. 5) obtained from the difference between the modified drag term, D^*, (Eq. 2) and the modified thrust term, T^*, (Eq. 4). This approach includes the terms of the fuselage as a reference of the whole aircraft.

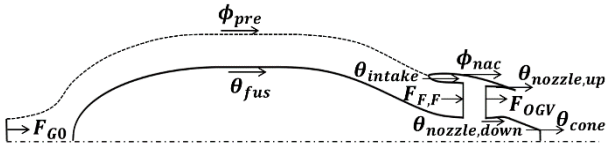

Figure 1: Control volume and force definition for the Modified Near-Field Method in a 2D axisymmetric propulsive fuselage

$$\phi_{pre} = -F_{G0} + F_{F,F} + \theta_{Intake} + \theta_{fus} \quad (1)$$

$$D^* = \phi_{pre} + \phi_{nac} \quad (2)$$

$$GPF^* = F_{OGV} - \theta_{nozzle,up} - \theta_{nozzle,down} - \theta_{cone} \quad (3)$$

$$T^* = -F_{G0} + GPF^* \quad (4)$$

$$NVF = D^* - T^* \quad (5)$$

2.2. Normalization of the NVF

The assessment of the aircraft performance by a thrust and drag accounting methodology determines the impact of the installation design. However, the NVF does not provide a way to compare different designs and their relative benefits. Hence, a strategy to evaluate the benefits of the BLI propulsor installation against the reference aircraft without BLI propulsor is established.

First, it is necessary to define the main reference values from the baseline aircraft: the reference thrust of the original installed aircraft, T_{ref}; and the sum of the overall drag of the airframe, defined as the Net Vehicle Force of the uninstalled reference aircraft, $NVF_{ref\text{-}ac}$. This methodology has to be adapted for the 2D axisymmetric case study of the present work. Therefore, the uninstalled aircraft airframe is modified to an axisymmetric design in order to obtain the corresponding $NVF_{ref\text{-}ac}$ value.

Following the work of Sanders [28], the value of the Relative Net Thrust Force, F_{RN}, (Eq. 6) is defined as the difference between the *NVF* of the BLI configuration and the reference uninstalled aircraft. This represents the thrust contribution from the BLI propulsor and its aerodynamic installation. An assumption is that the force on the airframe remains constant and any benefit or penalty comes only from the installation of the BLI propulsor.

$$F_{RN} = NVF - NVF_{ref-ac} \quad (6)$$

The value of the F_{RN} can be scaled with the value of the reference thrust to define the Thrust Split, *TS*, (Eq. 7). This parameter determines the propulsive performance at a whole aircraft level. The Thrust Split quantifies the amount of thrust that the BLI provides relative to the baseline.

$$TS = -\frac{F_{RN}}{T_{ref}} \quad (7)$$

The parameters that are used to define the performance of the BLI propulsor are the Thrust Specific Power Consumption, *TSPC*, (Eq. 8) and the propulsive efficiency, η_{prop}, (Eq. 9). Both values scale the Relative Net Thrust Force with the input power of the propulsive system, W_{prop}. This value is obtained from the integration of the energy flux

between the inlet and the exhaust boundaries of the propulsive system. Any internal loss on the fan control volume is represented by the fan isentropic efficiency. The propulsive efficiency is scaled with the value of the freestream velocity to keep a common reference value independently of the geometric design of the fuselage and the BLI propulsor intake.

$$TSPC = \frac{-W_{prop}}{F_{RN}} \quad (8)$$

$$\eta_{prop} = -V_{\infty}\frac{F_{RN}}{W_{prop}} \quad (9)$$

2.3. Intake performance

The intake performance has shown to be one of the possible limitations for the novel configurations [29,30]. The close integration of the propulsive systems leads to a higher distortion at the fan face that could cause engine performance issues and increased loads on the fan blades. Thus, it is essential to evaluate the intake conditions and performance for the design of these novel technologies. For this evaluation, a reference plane on the fuselage is defined at a selected location (Fig. 2). This plane is bounded by the fuselage surface and the edge of the capture streamtube. Additionally, a reference plane ahead of the fan face boundary is set to obtain the representative fan face values.

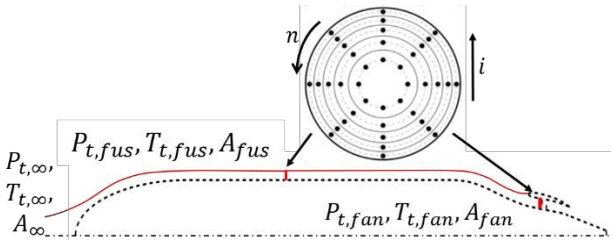

Figure 2: Rake distribution example on the reference planes

The metrics used for the intake performance are defined from established methodologies [31]. All the values are obtained by the definition of the equivalent of an experimental set-up (Fig. 2). Equally area spaced pressure rakes are distributed radially and azimuthally on the reference planes [30]. Area weighted total pressure is used to determine Intake Pressure Recovery, *IPR*, (Eq. 10) based on the freestream total pressure value, and the Ingested Intake Pressure Recovery, $IPR_{Ingested}$, (Eq. 11), based on the area weighted average of the total pressure on the fuselage reference plane. Radial Distortion Index, *RDI*, is applied as the main distortion descriptor (Eq. 12).

$$IPR = \frac{\overline{P_{t,fan}}}{P_{t,\infty}} \quad (10)$$

$$IPR_{Ingested} = \frac{\overline{P_{t,fan}}}{\overline{P_{t,fus}}} \quad (11)$$

$$RDI = max\left(\frac{\overline{P_{t,fan}}-\overline{P_{t,\iota=0}}}{\overline{q_{t,fan}}}, \frac{\overline{P_{t,fan}}-\overline{P_{t,\iota=N}}}{\overline{q_{t,fan}}}\right) \quad (12)$$

3. NUMERICAL APPROACH

3.1. Class Shape Transformations

The geometry is defined with Class Shape Transformation curves (CST) [5,21–23]. These curves have been shown to be suitable for the design of aerodynamic shapes [22,23]. The Class Shape transformation curve is a product of a Class Function (*C(ψ)*) and a Shape Function (*S(ψ)*) plus a parameter ($\Delta\xi_{te}$) which controls the trailing point offset (Eq. 13).

$$\xi(\varphi) = S(\varphi)C(\varphi) + \varphi\Delta\xi_{te} \;\; ; \;\; \xi = \frac{y}{c} \;\; ; \;\; \varphi = \frac{x}{c} \quad (13)$$

$$C_{N_2}^{N_1}(\varphi) = \varphi^{N_1}[1-\varphi]^{N_2} \quad for \quad 0 \le \varphi \le 1 \quad (14)$$

The class function cane be any function that has similar geometric properties to the desired CST curve. A common group of class functions are defined by Eq. 14, where changes to the exponents N_1 and N_2 result in different aerodynamic shapes such as a cone ($C_{0.+}^{1.0}$), an ellipse ($C_{0.5}^{0.5}$), biconvex ($C_{1.0}^{1.0}$), Sears Hack ($C_{0.75}^{0.75}$), and a round nosed airfoil ($C_{0.5}^{1.0}$)), [22]. The shape function is often comprised of Bernstein Polynomial equations (Eq. 15). The shape function and therefore the CST curve can be modified by the variation of Bernstein Polynomial coefficients (Eq. 16).

$$BP(\varphi) = \sum_{i=0}^{n}\left[K_{i,n}(\varphi^i(1-\varphi)^{n-1})\right] \;\; ; \;\; K_{i,n} = \frac{n!}{i!\,(n-1)!} \quad (15)$$

$$S(\varphi) = \textstyle\sum_{i=0}^{n}\left[bp_i K_{i,n}(\varphi^i(1-\varphi)^{n-1})\right] \quad (16)$$

However, controlling CST shapes by manipulating the Bernstein Polynomial coefficients is non-intuitive to the aerodynamic designer where there is no obvious link to familiar geometric or aerodynamic parameters. To overcome this drawback intuitive Class Shape Transformation (iCST) curves have been developed [5,21]. The iCST method allows the Bernstein Polynomial coefficients to be analytically calculated as a function of the imposed constraints. These constraints can take the form of a positional hard-point through which the curve must pass or an imposed n^{th} derivative at a specified ordinate. A linear set of equations (Eq. 17) can be constructed as in Eq. 17 where **A**, **B** and **X** are the matrices of coefficients, constant terms and solutions respectively. For every geometrical constraint imposed upon the curve an equation is added to the

linear set of equations (Eq. 17) which relates the constraint to the Bernstein Polynomial coefficients through Eq. 18 [5].

$$\boldsymbol{A} \cdot \boldsymbol{X} = \boldsymbol{B} \tag{17}$$

$$\xi^{(k)}(\varphi) = \left[\sum_{i=0}^{n}\left[bp_i K_{i,n}(\varphi^i(1-\varphi)^{n-1})\right]C(\varphi) + \varphi\Delta\xi_{te}\right]^{(k)} \tag{18}$$

The shape function and its derivatives can be solved by using the fact that derivatives of the k[th] degree Bernstein Polynomials are polynomials of degree k-1 and can be written as a linear combination of Bernstein Polynomials (Eq. 19) [5]. The solution of Equation 18 is then straightforward and Eq. 17 can then be inverted (Eq. 20) to solve for the Bernstein Polynomial coefficients.

$$\frac{d}{d\varphi}BP_{i,n}(\varphi) = n[BP_{k-1,n-1}(\varphi) - BP_{k,n-1}(\varphi)] \tag{19}$$

$$\boldsymbol{X} = \boldsymbol{A}^{-1}\boldsymbol{B} \tag{20}$$

3.2. Geometry parameterization

The aircraft fuselage axisymmetric definition (Fig. 3) was modelled without the use of CST. A cylindrical fuselage is applied with an elliptical nose geometry. The cylindrical fuselage is extended from the nose end to the beginning of the tapered rear fuselage. From this point, the iCST aft fuselage curve is defined with a zero degrees local slope constraint. The distance from the nose tip to the aft fuselage definition is defined as a fraction of the total length of the reference aircraft. The overall position of the fan hub (Fig. 3) is defined axially and radially from the shoulder of the aircraft.

Intuitive CST curves are used to define the intake, nacelle, exhaust and aft fuselage geometry. The intake geometry and the aft fuselage parameterizations are considered in the same group (Fig. 4a). The position of the system is defined with the hub location (l_{tc}, r_{hub}) and the length of the tail cone (l_{tail}). The aft fuselage curve (l_{tc}) is defined by controlling the local slope of the curve (θ_{curv}, θ_{ff}) at specific locations. A rotation of the intake geometry to orientate the design towards the flow has been implemented. The intake inclination parameter, Ω_{intake}, offsets the highlight position and changes the curvature distribution of the intake to maintain the desired area distribution. The rest of the parameters of the intake are modelled according to the definitions of Christie et al. [5]. Non-dimensional values for the parameters of the intake are defined to simplify the parametric inputs (Eqs. 22-25). The parameters allow a flexible definition of the intake geometry as well as the capability to orientate the installation towards the flow direction. This defined parameterization controls the intake throat area by imposing the required value through a rolling ball method.

$$AR_{int} = \frac{l_{int}}{2r_{fan}} \tag{22}$$

$$AR = \frac{l_{int} - l_{thr}}{r_{hi} - r_{thr}} \tag{23}$$

$$CR = \left(\frac{r_{hi}}{r_{thr}}\right)^2 \tag{24}$$

$$httr = \frac{r_{fan}}{r_{hub}} \tag{25}$$

The cowl parameterization (Fig. 4b) is based on the work of Heidebrecht et al. [6], while the exhaust is a simplification of the work of Goulos et al. [7]. The fan cowl is divided into two sections with independent iCST curves for the forebody and the afterbody of the profile. The curves are separated by the position of the nacelle maximum radius. This separation allows the combination of different afterbodies for a particular nacelle leading edge geometry [6,32].

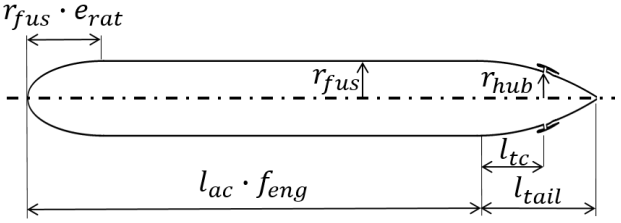

Figure 3: Parametric definition of the fuselage and engine position

The exhaust definition (Fig. 4b) has been simplified from the parameterization proposed by Goulos [7] for a single fan exhaust configuration without bypass flow. All the areas imposed on the parameterization are based on a rolling ball method. The exhaust geometry is initially constrained to provide a convergent exhaust system.

3.3. CFD domain and boundary conditions

A C-shaped domain (Fig. 5) is used for the 2D axisymmetric numerical analysis. The dimensions of the domain are defined as a function of the aircraft length and the radius of the fuselage. Different dimensions were tested to evaluate the influence of the domain on the metrics. The final domain size was determined after assuring no interference of the boundaries on the solution.

Far field boundary conditions are imposed at the domain extents by defining the flight altitude and Mach number. The static atmosphere conditions are defined by using the ISA model [33]. The surfaces of the aircraft and the BLI propulsor installation were defined as non-slip wall conditions. The boundaries of the propulsive system were defined to emulate a single stage fan and outlet guided vanes (OGV).

Based on the standards of this configuration the propulsive system is assumed to be electrically or turbo-electrically driven [15,34]. The fan face is modelled with a target mass flow inlet selected for a specific amount of boundary layer ingestion. The OGV outlet plane is modelled with a pressure inlet boundary condition with the total temperature and pressure values obtained from the fan cycle, determined by the fan pressure ratio and the fan isentropic efficiency.

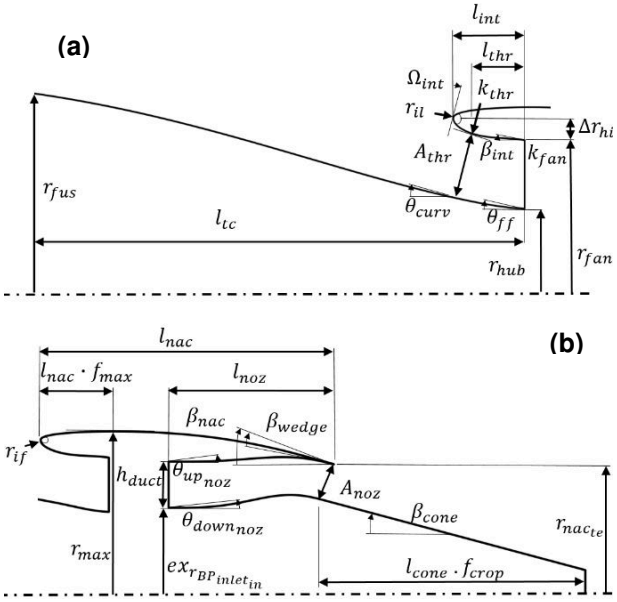

Figure 4: Geometry parameterization: (a) Intake and fuselage aft curve, and (b) fan cowl and exhaust

A consistent value of the mass flow ratio between the fan face and the OGV boundary is required to ensure modelling coherence. The pressure inlet boundary condition at the OGV outlet cannot always provide the needed value of the mass flow rate for a given exhaust geometry, fan properties, and flight conditions. The geometry of the nacelle, combined with the local aerodynamics affects the effective value of the static pressure at the exhaust exit. Hence, it is necessary to modify the total pressure and temperature values on the OGV boundary condition to match the target mass flow. These values of the total pressure and temperature are obtained by applying a constant isentropic efficiency of the fan and correcting the value of the FPR with an iterative method to match the target mass flow. This methodology was implemented using an ANSYS FLUENT user defined function [35].

3.4. Mesh and topology definition

An automatic structured grid generation methodology has been implemented using the commercially available meshing tool ANSYS ICEM CFD [36]. The mesh is generated with a reference value for the axial discretization and a target value for the y^+ with the prescribed boundary conditions. This methodology was designed to be consistent with multiple designs and propulsive system positions around the fuselage. The grid is designed with a multi-block strategy to define the main characteristics of the case study.

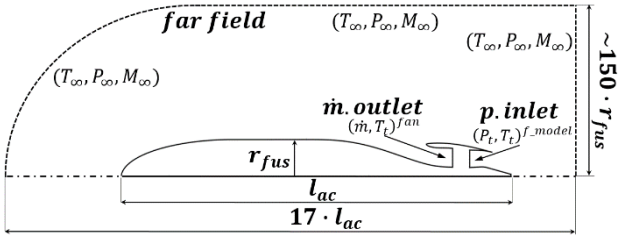

Figure 5: CFD domain and boundary conditions

3.5. CFD methodology

A Favre Averaged Navier-Stokes density based numerical approach was used [37]. The *k-ω* shear-stress transport turbulence [38] closure model was used. The appropriateness of this model was based on previous work on the analysis of the aerodynamic installation of propulsion systems [7,32].

A Green-Gauss cell based method is applied for the computation of the gradients of the flow field. A second-order upwind scheme is utilized for the spatial discretization. An ideal gas model is applied and the gas thermodynamic properties are defined by the kinetic theory. For the definition of the dynamic viscosity, Sutherland's law is employed.

3.6. Optimization

The developed framework has the capability for multi-objective optimization (MOO) studies using evolutionary algorithms. The design of experiments is initiated with a Latin Hypercube Sampling (LHS) [39] to efficiently cover the relatively high-dimensional space investigated with the tool. The Non-dominated Sorted Genetic Algorithm II (NSGA-II), originally developed by Deb et al. [40], is use due to its global optimization characteristics for transonic flow aerodynamic applications [41]. The hyper-parameters of the genetic algorithm were adjusted to ensure a fast convergence to the Pareto front while ensuring diversity within the optimal set of solutions. The mutation standard deviation size was set to 0.0005 to obtain the best compromise between convergence speed and reduction on the risk to be trapped in a local optimum [42]. The crossover uses the BLX-α operator with α = 0.5 due to the demonstrated convergence capabilities for a wide range of benchmark test functions [43].

4. RESULTS AND DISCUSSION

4.1. Grid sensitivity analysis

A grid sensitivity analysis was carried to determine the dependency of the solutions with the mesh discretization. Sample cruise conditions (Tab. 1) of a medium-sized single-aisle aircraft were applied. Fan nominal conditions corresponded to a low thrust contribution BLI propulsor [11]. The mass flow is selected for a boundary layer ingestion rate (BLR) of the 40% of the boundary layer height [34] at a reference station of the fuselage (Fig. 2)

Table 1: BLI operating conditions for the grid sensitivity study

Cycle parameter	Value	Unit
FPR	1.3	-
Altitude	32,000	ft
M_∞	0.78	-
BLR	0.4	-

Table 2: Grids used for the Grid Sensitivity Index calculation

Mesh	A	B	C
Elements ($\times 10^3$)	196.93	443.09	996.94

Table 3: Grid Convergence Index for the different metrics of the study

GCI (%)	A-B	B-C
NVF	1.727	0.329
IPR	0.509	0.209
RDI	0.236	0.037
C^*_V	0.00461	0.00115

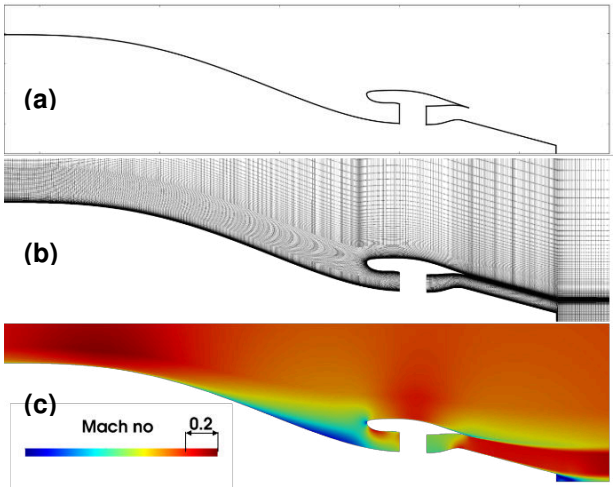

Figure 6: Design selected for the grid sensitivity analysis: (a) geometry of the model, (b) Mesh B, 4.43×10^5 elements, and (c) Mach number contour

Six meshes were applied for the analysis. The refinement was increased progressively. A scaling factor for the mesh density was used to keep a uniform refinement. The number of elements varied from approximately 1.3×10^5 to 9.97×10^5 quadrilateral elements. All the meshes had a value of y^+ of approximately 1.0. The distortion metrics, the NVF and exhaust performance metrics as the C^*_V and C_D [7] were analysed. Monotonic behaviour was observed for all the meshes of the study with a breakpoint after the fourth mesh with 4.43×10^5 elements.

The nature of the numerical discretization was addressed with the Grid Convergence Index (GCI) [44]. Three of the meshes (Tab. 2) were used for this analysis. The main performance metrics for the BLI propulsor, intake and exhaust were evaluated (Tab. 3). Mesh B (Fig. 6) discretization was chosen for the present approach and all the future calculations.

4.2. Design Space Exploration

An exploration of the aerodynamic installation design space was carried to determine the impact of the parameters on the main performance metrics and its correlation. Cruise conditions (Tab. 1) were applied for the study. The propulsor radial and axial location, and fan area were fixed. Only the intake (Fig. 4a) and fan cowl (Fig. 4b) parameters were modified. A fixed exhaust geometry is applied (Fig. 7). The nacelle trailing edge position was fixed, but the boat-tail angle was allowed to change to fit the nacelle designs.

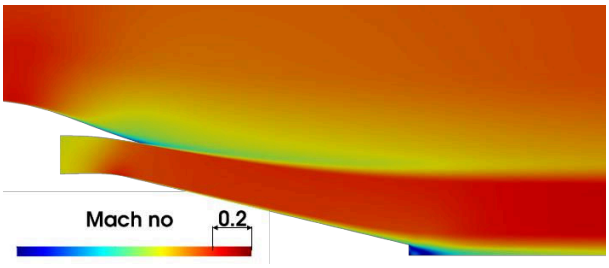

Figure 7: Fixed exhaust design for the design space exploration

LHS [39] was applied to populate the parameters for a selected range. For some parameter combinations, the CST methodology allows the generation of curves with undesirable features such as inflected fan cowls and multiple throat points on the intake. A geometry filter was used to avoid inadequate geometric characteristics and to limit the computational effort. The fan cowl leading edge curve is required to be concave ($\xi''(\varphi)<0$ for $\varphi\in(0,1)$), so no inflection points were accepted. On the fan cowl afterbody, one inflection point was tolerated to avoid overconstraining the design

space. The intake curve is expected to change from concave to convex ($\xi''(\varphi)>0$ for $\varphi\in(\varphi_{inf},1)$ between the throat and the fan face. Thus, the number of inflection points on the curve was limited to one. Additionally, a maximum fan face Mach number condition was applied.

After filtering, 290 designs were available for the study of the design space. The BLI propulsor performance metrics *TS* and TSPC have an inverse power law relationship between them (Eq. 26). The input power of the propulsive system varies with the FPR, which is modified to match the fan mass flow. Both metrics (Fig. 8a) show a very strong linear correlation [45] between their logarithms with a strong monotonic behaviour. The correlation values obtained from the logarithmic values with that level of monotonicity suggest that the metrics can be still be correlated with the inverse power law accounting for the power variation. The intake performance metrics (Fig. 8b) show a very strong negative linear correlation [45] with a good level of monotonicity. The momentum-based performance metrics do not show any correlation or monotonic behaviour with the intake performance metrics (Fig. 8c). The weak correlation level between the different groups suggests that the analysis of the momentum-based performance can be separated from the intake performance by modifying the appropriate parameters. This low level of correlation can be used to choose suitable non-conflicting objective functions for Multi-Objective Optimizations.

$$TSPC = \frac{W_{prop}}{T_{ref}}\frac{1}{TS} \tag{26}$$

The correlation of the parameters with the performance metrics was addressed (Fig. 9). The individual correlation and monotonicity of each of the parameters used for the DSE show the inverse behaviour between the *TSPC* and *TS*, and between the $IPR_{Ingested}$ and *RDI.* This is a reflection of the negative correlation and monotonicity between each group of metrics (Fig. 9). The parameters that show a higher correlation with the momentum and energy based performance are the parameters directly related to the fan cowl geometry. The location of the maximum radius, f_{max}, and the maximum radius value, r_{max}, have a moderate and strong negative linear correlation with *TS*, respectively, with a stronger value of the monotonicity. This is because flatter nacelles with a location of the maximum radius closer to the leading edge have a less negative impact on the thrust performance. Other parameters that may affect the fan cowl performance are the highlight radial position, r_{hi}, the boat-tail angle, β_{nac}, or the intake inclination do not show direct correlation or monotonic behaviour with the momentum and power based performance metrics.

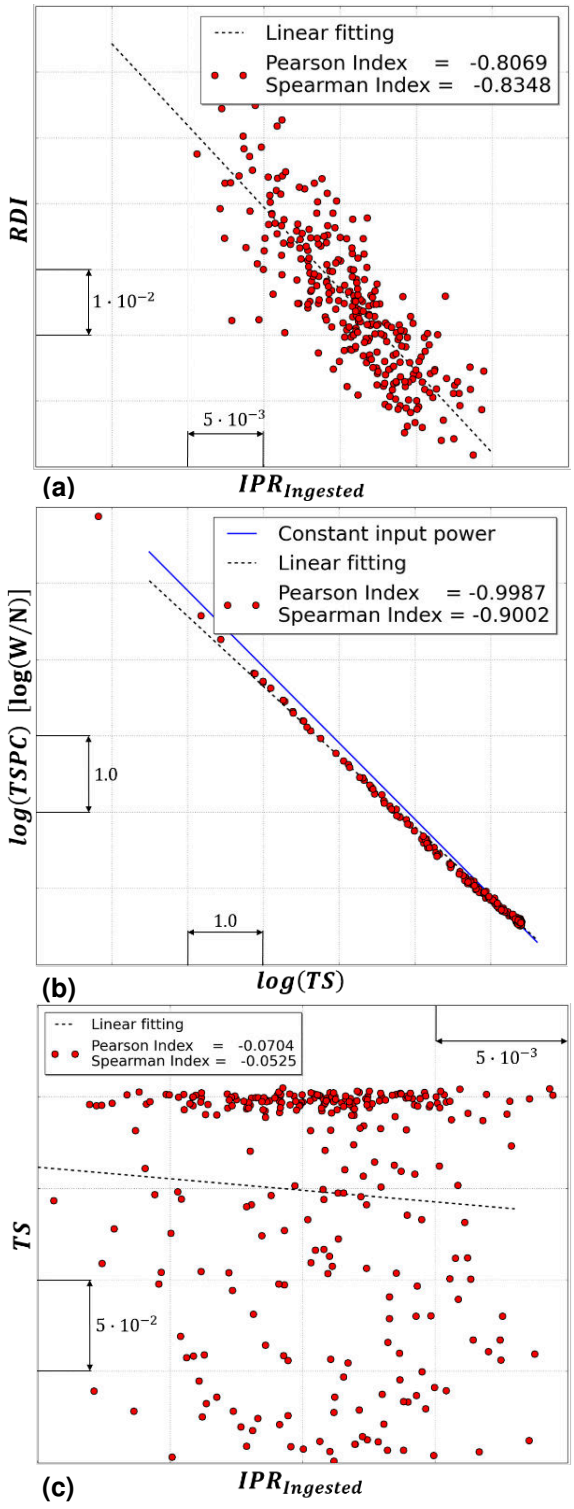

Figure 8: Correlation of the performance metrics of the DSE: (a) Intake performance metrics, (b) momentum and power based metrics, and (c) intake and momentum based performance metrics

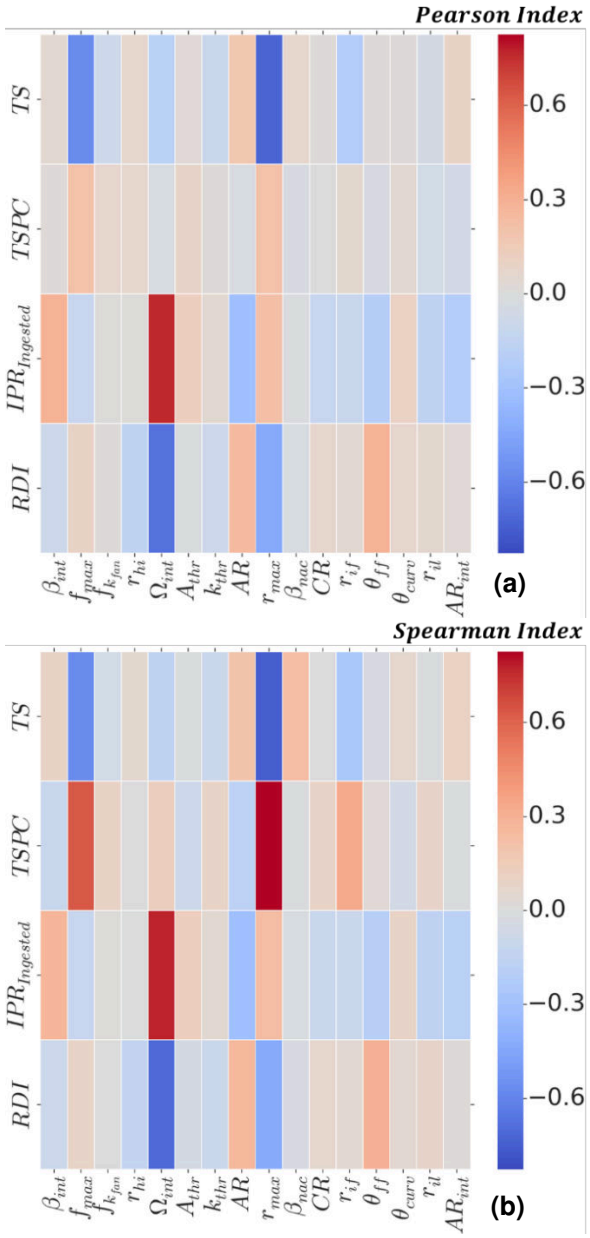

Figure 9: Correlation between the parameters of the DSE and the main performance metrics: (a) Pearson Index linear correlation, and (b) Spearman Index monotonicity assessment

The intake performance is mainly influenced by the intake and aft fuselage curve geometry. The intake inclination, Ω_{intake}, and the slope angle at the fan tip, β_{int}, have a strong and moderate positive correlation, respectively, with a good monotonicity with $IPR_{Ingested}$ and a similar negative behaviour with *RDI*. This indicates potential benefits of an increase in the angle of the nacelle to orientate towards the flow over the tail cone. Compared with the intake geometry, the correlation between the intake performance metrics and the parameters of the aft fuselage curve shows a different behaviour. The area of the throat, A_{thr}, has a moderate negative correlation and monotonicity with the *RDI* while the angle of the slope at the fan hub position, θ_{ff}, has a moderate positive correlation and monotonicity with the *RDI*. Additionally, the aspect ratio, *AR,* has a moderate positive linear correlation with the *RDI.* The combination of the three parameters indicates that a less aggressive aft fuselage local slope towards the fan is required to reduce the distortion levels, mainly on the part of the aft fuselage curve inside the intake.

4.3. Optimization

For this investigation, the radial and axial location of the propulsor were fixed, as well as the fan frontal area and exhaust geometry (Fig. 7). Sample cruise conditions were applied (Tab. 1). A total of 16 degrees of freedom were used to define the fan cowl, intake and aft fuselage curve geometries (Fig. 3). The *TS* (Eq. 7) and the $IPR_{Ingested}$ (Eq. 11) were applied as objective functions to evaluate the intake and the system aerodynamic performance. The optimization was started with an initial population size of around 600 individuals using LHS [39]. The maximum number of generations was set to 30 with a maximum of 96 designs on each generation.

The geometry was filtered to avoid incompatible geometry definitions of the iCST curves. The nacelle forebody curve was constrained to be concave ($\xi''(\varphi)<0$ for $\varphi\in(0,1)$) not allowing any inflection point on the curve. On the nacelle afterbody, a maximum of one inflection point was allowed. On the intake curve, it is expected a change from concave to convex ($\xi''(\varphi)>0$ for $\varphi\in(\varphi_{inf},1)$) between the throat and the fan face. Thus, the number of inflections was limited to one. Additionally, a maximum Mach number constrain on the fan face was applied.

For the evaluation of the optimization capability, one reference design was introduced (DES-0). The limitations of the aerodynamic installation design with the defined constraints are defined by the non-dominated designs of the Pareto front (Fig. 10). A maximum improvement from the DES-0 of approximately the 0.425% is expected on the value of the $IPR_{Ingested}$. The *TS* can improve up to a 2% from the DES-0. The *TS* improvement from the DES-0 describes a benefit of close to a 0.4% of the reference aircraft thrust, only with a redesign of the propulsor installation.

Three non-dominated geometries (Fig. 11) were chosen to outline the characteristics of the obtained designs. The local slope of the fuselage aft curve on the intake region has an important effect on the

intake performance. The improvement of the intake performance is also linked with the increase of the intake inclination. The intake inclination at the same time produces a penalty on the pressure force contribution to the *TS* (Design A). A reduction of the nacelle length is present on the three selected designs to compensate the exposed area increase. Additionally, the intake inclination can be used to obtain additional thrust contribution on the fan cowl with the modification of the nacelle afterbody (Designs B and C).

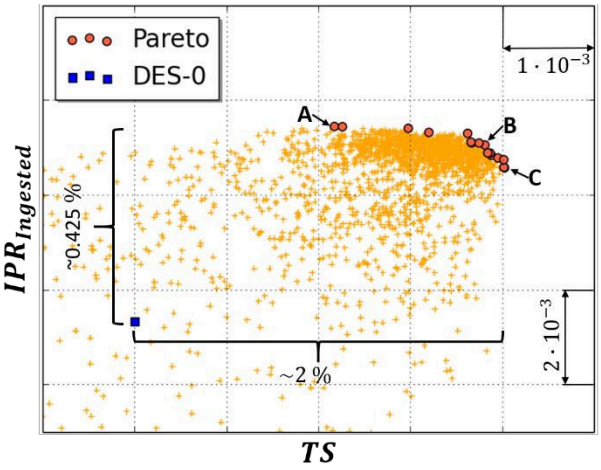

Figure 10: Designs evaluated on the multi-objective optimization

5. CONCLUSIONS

A systematic automated approach for the design of a BLI propulsive fuselage configuration has been developed. This approach comprises geometry generation, an automatic aerodynamic numerical computation with a compressible viscous solver, and an aircraft and propulsive system aerodynamic installation performance evaluation. This approach had to face new challenges coming from the novel aircraft configurations by using current state of the art design methodologies adapted to these new characteristics.

The application of the methodology has been demonstrated for an example of an embedded annular propulsor. An intuitive parameterization of the geometry has been developed for each element of the installation. The geometry is generated by using intuitive Class Shape Transformations. An automated computational approach with a density-based solver for the RANS equations has been implemented.

A design space exploration for a given propulsor location was conducted. The proposed metrics for the performance evaluation were analysed to determine their impact on the installation aerodynamics. Also, the correlation between the parameters and the performance metrics was addressed to identify viable design space possibilities.

Finally, a multi-objective optimization was carried to demonstrate the capabilities of the automated approach. Fan cowl and intake geometries were optimized with a fixed propulsor location and exhaust geometry. The optimization results revealed that relevant aerodynamic performance improvements can be obtained with the redesign of the propulsor aerodynamic installation.

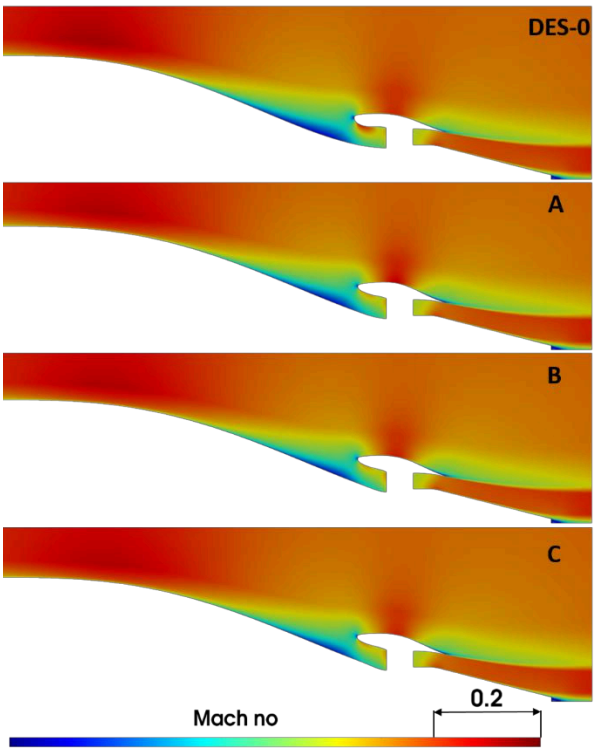

Figure 11: Mach number contours for the selected Pareto designs

REFERENCES

1. ACARE. (2011). Flightpath 2050. Europe's Vision for Aviation. *European Union.* doi:10.2777/50266.
2. Dae Kim, H. (2010). Distributed Propulsion Vehicles. *27th International Congress of the Aeronautical Sciences, ICAS*
3. Gohardani, A. S., Doulgeris, G., & Singh, R. (2011). Challenges of Future Aircraft Propulsion: A Review of Distributed Propulsion Technology and Its Potential Application for the All Electric Commercial Aircraft. *Progress in Aerospace Sciences*, Vol. 47, No. 5, pp. 369–391. doi:10.1016/j.paerosci.2010.09.001.
4. Steiner, H.-J., Seitz, A., Wieczorek, K., Plötner,

K., Isikveren, A. T., & Hornung, M. (2012).Multi-Disciplinary Design and Feasibility Study of Distributed Propulsion Systems. *28th International Congress of the Aeronautical Sciences (ICAS).* doi:10.1016/S0092-1157(78)80007-9.

5. Christie, R., Heidebrecht, A., & MacManus, D. (2017). An Automated Approach to Nacelle Parameterization Using Intuitive Class Shape Transformation Curves. *Journal of Engineering for Gas Turbines and Power*, Vol. 139, No. 6. doi:10.1115/1.4035283.
6. Heidebrecht, A., Stankowski, T., & MacManus, D. (2016) Parametric Geometry and CFD Process for Turbofan Nacelles. *Proceedings of ASME 2016 Turbo Expo: Turbomachinary Technical Conference and Exposition*, No. GT2016-57784.
7. Goulos, I., Stankowski, T., Otter, J., MacManus, D., Grech, N., & Sheaf, C. (2016).Aerodynamic Design of Separate-Jet Exhausts for Future Civil Aero-Engines - Part I: Parametric Geometry Definition and Computational Fluid Dynamics Approach. *Journal of Engineering for Gas Turbines and Power*, Vol. 138, No. 8. doi:10.1115/1.4032649.
8. Rodriguez, D. L. (2009). Multidisciplinary Optimization Method for Designing Boundary-Layer-Ingesting Inlets. *Journal of Aircraft*, Vol. 46, No. 3, pp. 883–894. doi:10.2514/1.38755.
9. Kim, H., & Liou, M. S. (2013). Shape Design Optimization of Embedded Engine Inlets for N2B Hybrid Wing-Body Configuration. *Aerospace Science and Technology*, Vol. 30, No. 1, pp. 128–149. doi:10.1016/j.ast.2013.07.011.
10. Kenway, G. K. W., & Kiris, C. (2018). Aerodynamic Shape Optimization of the STARC-ABL Concept for Minimal Inlet Distortion. *AIAA/ASCE/AHS/ASC Structures, Structural Dynamics, and Materials Conference,* No. 210049, 2018. doi:10.2514/6.2018-1912.
11. Gray, J. S., Mader, C. A., Kenway, G. K. W., & Martins, J. R. R. A. (2018). Modeling Boundary Layer Ingestion Using a Coupled Aeropropulsive Analysis." *Journal of Aircraft*, Vol. 55, No. 3, pp. 1191–1199. doi:10.2514/1.C034601.
12. Felder, J., Kim, H., Brown, G., & Kummer, J. (2011). An Examination of the Effect of Boundary Layer Ingestion on Turboelectric Distributed Propulsion Systems. *49th AIAA Aerospace Sciences Meeting including the New Horizons Forum and Aerospace Exposition*, No. January, pp. 1–26. doi:10.2514/6.2011-300.
13. Wiart, L., Atinault, O., Grenon, R., Paluch, B., & Hue, D. (2015). Development of NOVA Aircraft Configurations for Large Engine Integration Studies.
14. Seitz, A., & Gologan, C. (2014). Parametric Design Studies for Propulsive Fuselage Aircraft Concepts. *CEAS Aeronautical Journal*, Vol. 6, No. 1, pp. 69–82. doi:10.1007/s13272-014-0130-3.
15. Seitz, A., Peter, F., Bijewitz, J., Habermann, A., Goraj, Z., Kowalski, M., Pardo, A. C., Hall, C., Meller, F., Merkler, R., Petit, O., Samuelsson, S., Corte, B. Della, Sluis, M. Van, Wortmann, G., & Dietz, M. (2018). CONCEPT VALIDATION STUDY FOR FUSELAGE WAKE- FILLING PROPULSION INTEGRATION. *31st Congress of the International Council of the Aeronautical Sciences, ICAS*.
16. Felder, J. L. (2014). NASA N3-X with Turboelectric Distributed Propulsion. *IMechE Disruptive Green Propulsion Technologies conference*.
17. Hall, D. K., Huang, A. C., Uranga, A., Greitzer, E. M., Drela, M., & Sato, S. (2017). Boundary Layer Ingestion Propulsion Benefit for Transport Aircraft. *Journal of Propulsion and Power*, Vol. 33, No. 5, pp. 1118–1129. doi:10.2514/1.B36321.
18. Uranga, A., Drela, M., Hall, D. K., & Greitzer, E. M. (2018). Analysis of the Aerodynamic Benefit from Boundary Layer Ingestion for Transport Aircraft. *AIAA Journal*, Vol. 56, No. 11, pp. 4271–4281. doi:10.2514/1.J056781.
19. Smith, L. H. (1993). Wake Ingestion Propulsion Benefit. *Journal of Propulsion and Power*, Vol. 9, No. 1, pp. 74–82. doi:10.2514/3.11487.
20. Blumenthal, B. T., Elmiligui, A. A., Geiselhart, K. A., Campbell, R. L., Maughmer, M. D., & Schmitz, S. (2018). Computational Investigation of a Boundary-Layer-Ingestion Propulsion System. *Journal of Aircraft*, Vol. 55, No. 3, pp. 1–13. doi:10.2514/1.C034454.
21. Zhu, F., & Qin, N. (2014). Intuitive Class/Shape Function Parameterization for Airfoils. *AIAA Journal*, Vol. 52, No. 1, pp. 17–25. doi:10.2514/1.J052610.
22. Kulfan, B., & Bussoletti, J. (2006).'Fundamental' Parameteric Geometry Representations for Aircraft Component Shapes. *11th AIAA/ISSMO Multidisciplinary Analysis and Optimization Conference*, No. September, pp. 1–45. doi:10.2514/6.2006-6948.
23. Kulfan, B. M. (2008). Universal Parametric

Geometry Representation Method. *Journal of Aircraft*, Vol. 45, No. 1 , pp. 142–158. doi:10.2514/1.29958.

24. Drela, M. (2009).Power Balance in Aerodynamic Flows. *AIAA Journal*, Vol. 47, No. 7, pp. 1761–1771. doi:10.2514/1.42409.
25. Uranga, A., Drela, M., Greitzer, E., Titchener, N., Lieu, M., Siu, N., Huang, A., Gatlin, G. M., & Hannon, J. (2014). Preliminary Experimental Assessment of the Boundary Layer Ingestion Benefit for the D8 Aircraft. *52nd Aerospace Sciences Meeting*, No. January, pp. 1–25. doi:10.2514/6.2014-0906.
26. Arntz, A., & Atinault, O. (2015). Exergy-Based Performance Assessment of a Blended Wing–Body with Boundary-Layer Ingestion. *AIAA Journal*, Vol. 53, No. 12, pp. 3766–3776. doi:10.2514/1.J054072.
27. MIDAP Study group. (1979). *Guide to In-Flight Thrust Measurement of Turbo- Jets and Fan Engines. Agardograph No. 237, Technical Report No. AG-237*. Neuilly sur Seine, France.
28. Sanders, D. (2018). *Boundary Layer Ingestion Performance Assessment with Application to Bussines Jets*. PhD Thesis, School of Aerospace, Transport and Manufacturing, Centre for Propulsion Engineering, Cranfield University.
29. Lee, B. J., Liou, M. S., & Kim, C. (2009). Adjoint Based Design Approach for Boundary Layer Ingestion Offset Intake. *19th AIAA Computational Fluid Dynamics Conference*, No. June, pp. 1–19. doi:10.2514/6.2009-3804.
30. MacManus, D. G., Chiereghin, N., Gil Prieto, D., & Zachos, P.(2015). Complex Aero-Engine Intake Ducts and Dynamic Distortion. No. June, pp. 1–28. doi:10.2514/6.2015-3304.
31. S-16 Turbine Engine Inlet Flow Distortion Committee. (1999). *Inlet Total-Pressure-Distortion Considerations for Gas-Turbine Engines. No. AIR1419*. USA.
32. Tejero, F., Robinson, M., MacManus, D. G., & Sheaf, C. (2019). Multi-Objective Optimisation of Short Nacelles for High Bypass Ratio Engines. *Aerospace Science and Technology*, Vol. 91, pp. 410–421. doi:10.1016/j.ast.2019.02.014.
33. ISO International Standard 2533-1975. (1978). *Standard Atmosphere First Edition*. Geneva, Switzerland.
34. Welstead, J. R., & Felder, J. L. (2016). Conceptual Design of a Single-Aisle Turboelectric Commercial Transport with Fuselage Boundary Layer Ingestion. *54th AIAA Aerospace Sciences Meeting*. doi: 10.2514/3.12149
35. ANSYS INC. (2013). *ANSYS Fluent UDF Manual. Release 15.0*. Canonsburg, PA, USA.
36. ANSYS INC. (2013). *ANSYS ICEM CFD User Manual*. Canonsburg, PA, USA.
37. ANSYS INC. (2013). *ANSYS Fluent User's Guide. Release 15.0*. Canonsburg, PA, USA.
38. Menter, F. R. (1994). Two-Equation Eddy-Viscosity Turbulence Models for Engineering Applications. *AIAA Journal*, Vol. 32, pp. 1598–1605. doi: 10.2514/3.12149
39. Helton, J. C., & Davis, F. J. (2003). Latin Hypercube Sampling and the Propagation of Uncertainty in Analyses of Complex Systems. *Reliability Engineering and System Safety*, Vol. 81, No. 1, pp. 23–69. doi:10.1016/S0951-8320(03)00058-9.
40. Deb, K., Member, A., Pratap, A., Agarwal, S., & Meyarivan, T. (2002). A Fast and Elitist Multi-Objective Genetic Algorithm:NSGAII. Vol. 6, No. 2, pp. 182–197.
41. Tejero, F., MacManus, D. G., & Sheaf, C. (2019). Surrogate-Based Aerodynamic Optimisation of Compact Nacelle Aero-Engines. *Aerospace Science and Technology*, Vol. 93, p. 105207. doi:10.1016/j.ast.2019.05.059.
42. Robinson, M., MacManus, D. G., Heidebrecht, A., & Grech, N. (2017). An Optimization Method for Nacelle Design. *AIAA SciTech Forum - 55th AIAA Aerospace Sciences Meeting*, No. January, 2017, pp. 1–17. doi:10.2514/6.2017-0708.
43. Eshelman, L . J. , & Schaffer, J. (1993). Real-Coded Genetic Algorithms and Interval-Schemata. *Found. Genet. Algorithms*, Vol. 2, pp. 187–202.
44. Celik, I. B., Ghia, U., Roache, P. J., Freitas, C. J., Coleman, H., & Raad, P. E. (2008). Procedure for Estimation and Reporting of Uncertainty Due to Discretization in CFD Applications. *Journal of Fluids Engineering, Transactions of the ASME*, Vol. 130, No. 7, pp. 0780011–0780014. doi:10.1115/1.2960953.
45. Evans, J. D. (1996). *Straightforward Statistics for the Behavioural Sciences*. Pacific Grove, California.